Astronomy Letters, Vol. 26, No. 3, 2000, pp. 144–152. Translated from Pis'ma v Astronomicheskiĭ Zhurnal, Vol. 26, No. 3, 2000, pp. 180–189.
Original Russian Text Copyright © 2000 by Babkovskaya, Varshalovich.

A Model for the Molecular Accretion Disk and H_2O Maser in the Nucleus of the Galaxy NGC 4258

N. S. Babkovskaya* and D. A. Varshalovich

Ioffe Physicotechnical Institute, Russian Academy of Sciences, ul. Politekhnicheskaya 26, St. Petersburg, 194021 Russia

Received September 24, 1999

Abstract—A model is developed for the H_2O maser source observed in the circumnuclear region of the galaxy NGC 4258. The maser emission originates at distances of 0.15–0.29 pc from the center in a thin, cold accretion disk (gas–dust torus) rotating around a supermassive black hole of mass $4 \times 10^7\ M_\odot$. The conditions for the emergence of an inverse population of the signal 6_{16}–5_{23} levels in ortho-H_2O working molecules are simulated numerically. The complex line profile, which includes both central and high-velocity components, is calculated. A comparison of the calculations with radiointerferometric and spectrophotometric observations allowed the physical conditions in the emitting region to be determined. *© 2000 MAIK "Nauka/Interperiodica".*

Key words: *active galactic nuclei, quasars, radio galaxies*

INTRODUCTION

Considerable progress in elucidating the nature of active galactic nuclei has become evident in connection with a radiointerferometric study of the H_2O maser emission from the nuclear region of the giant spiral SABbc galaxy NGC 4258 (M 106) located at distance $D = 7.3 \pm 0.3$ Mpc [1]; Miyoshi *et al.* [2] obtained a different estimate, $D = 6.4 \pm 0.9$ Mpc. The galaxy has a complex structure with inner and outer spiral arms [3], a dust lane, and jets, which are observed both in the optical (Hα) and radio ranges. By the characteristic appearance of its optical spectrum, NGC 4258 was initially classified as a Seyfert 2 galaxy or, more precisely, as Sy 1.9. Subsequently, it was classified as belonging to the subgroup of the so-called LINERs (Low Ionization Nuclear Emission Region). The total luminosity L of the nucleus of this galaxy is 10^{42}–$10^{44} L_\odot$ erg s^{-1} [4]. Since the galaxy nucleus itself is completely obscured by a gas–dust disk, $A_V > 100$, it can be observed optically only in scattered, linearly polarized light [4]. Accordingly, the emission as viewed by the observer is mainly concentrated in the near infrared. However, X-ray emission with a luminosity of $(4.4 \pm 1.1) \times 10^{40}$ $(D/7.3\ \text{Mpc})^2$ erg s^{-1} was detected in the 3–10-keV band [1].

NGC 4258 is unique in that the line of sight lies virtually in the plane of the molecular gas–dust accretion disk. That is why we can observe the maser emission from the disk. In this study, an attempt is made to restore the structure of the accretion disk by comparing observational data with calculations of the intensity of the maser emission. We were able to do this, because both the intensity and the spectral line profile are highly sensitive, first, to the number density and temperature of the H_2O working molecules and H_2 buffer gas and, second, to the geometry of the system and the gas velocity field, whose gradient determines the amplification path length before the emergence from resonance, 10^{14}–10^{15} cm.

The H_2O maser emission from the nucleus of NGC 4258 was first detected by Claussen *et al.* [5]; however, the first spectra were obtained in a narrow range of frequencies (velocities) corresponding to the central, most intense components of the maser line. Only a decade later did Nakai *et al.* [6] measure the spectrum in a wider frequency range and detected high-velocity components to the right and to the left of the central line (Fig. 1). Three hypotheses about the nature of the high-velocity components of maser emission were proposed: (a) a bipolar jet, (b) nonlinear scattering in a dense plasma, and (c) a molecular disk [6]. The nature of these components was finally elucidated only after VLBI measurements, which yielded a high-angular-resolution map of the spatial distribution of maser subsources [2].

An analysis of the interferogram revealed that the high-velocity components of the maser line arise in the right and left wings of a thin molecular disk (gas–dust torus) seen edge-on. The inclination i_0 of the disk spin axis to the line of sight is $97° \pm 4°$. Moreover, the maser features turned out to fall nicely on the Keplerian radial-velocity (V_s) curve

$$V_s - V_0 = \sqrt{\frac{GM}{R}} \sin i_0 \sin\theta, \qquad (1)$$

where θ is the angle between the direction of observation and the velocity vector of the maser region: $\theta = 0° \pm 3°$ for the central component of the maser line and $\theta = 90° \pm 4°$ for the high-velocity components, R is the

* E-mail address for contacts: bns@astro.ioffe.rssi.ru

radius of the Keplerian orbit, and V_0 is the apparent recession velocity of the disk [7].

The maximum and minimum rotation velocities of the maser features are $V_{max} = 1080 \pm 2$ km s^{-1} and $V_{min} = 770 \pm 2$ km s^{-1}, the radius R_{in} of the inner maser subsource corresponding to V_{max} is 0.15 pc (D/7.3 Mpc), whereas the radius R_{out} of the outer subsource corresponding to V_{min} is 0.29 pc (D/7.3 Mpc) [2] (Fig. 1). Owing to these measurements, the central mass inside the disk was determined for the first time with a high accuracy: $M = (4.0 \pm 0.25) \times 10^7 M_\odot$ (D/7.3 Mpc) [1]. The only explanation for the existence of such a large mass in such a small region is the presence of a supermassive black hole.

According to radio observations, the velocity V_0 of the maser disk with respect to the Local Standard of Rest (LSR) is 476 ± 2 km s^{-1} [8]. It includes the galaxy's cosmological recession velocity of 470 km s^{-1}, a gravitational redshift $GM/(Rc) \sim 4$ km s^{-1}, and a shift $GM/(2Rc) \sim 2$ km s^{-1} associated with the transverse Doppler effect. The velocity V_0 measured in the heliocentric coordinate system is lower by 8.2 km s^{-1} [7].

An upper limit on the maser-disk mass, $M < 4 \times 10^6 M_\odot$, was derived from the deviation of $V_s(R)$ from the Keplerian curve; the accretion rate is $\dot{M} = 1.5 \times 10^{-4} M_\odot$ yr^{-1} [1]; the radial velocity of the disk gas, as inferred from observational data, does not exceed 10 km s^{-1} [2].

THE MASER PUMPING MECHANISM

To calculate the populations n_k of energy levels ε_k in the ortho-H_2O molecule, we used the set of population balance equations, which includes all possible collisional and radiative transitions between the first thirty rotational levels of ortho-H_2O,

$$\sum_k n_k W_{ki} = n_i \sum_k W_{ik} \tag{2}$$

with the normalization condition

$$\sum_k n_k = n_{H_2O}, \tag{3}$$

where $i = 1, 2, \ldots, n_{H_2O}$ is the number density of water molecules, $W_{ik} = C_{ik} + R_{ik}$ is the total rate of the $i \longrightarrow k$ transition,

$$C_{ik}^{\uparrow} = n_{H_2} k_{ik}(T_{kin}), \quad C_{ki}^{\downarrow} = C_{ik}^{\uparrow} \frac{g_i}{g_k} \exp\left(\frac{\varepsilon_k - \varepsilon_i}{kT_{kin}}\right) \tag{4}$$

are the rates of collisional excitation $i \longrightarrow k$ and deexcitation $k \longrightarrow i$ ($\varepsilon_k > \varepsilon_i$), g_i is the statistical weight, n_{H_2} and T_{kin} are the number density and temperature of the H_2 buffer gas,

$$R_{ik}^{\uparrow} = \int A_{ik} \rho_{ik} \frac{d\Omega}{4\pi}, \quad R_{ki}^{\downarrow} = \int A_{ki}(1 + \rho_{ki}) \frac{d\Omega}{4\pi}, \tag{5}$$

are the rates of radiative excitation $i \longrightarrow k$ and deexcitation $k \longrightarrow i$, $A_{ik} = g_k/g_i A_{ki}$ are the Einstein coefficients determining the probability of a spontaneous transition, $\rho(\nu, \mathbf{n}) = I(\nu, \mathbf{n})c^2/2h\nu^3$ is a dimensionless intensity of the emission (the number of photons in a cell of phase space), and $\mathbf{n}$ is the direction of propagation of the emission. Collisional excitation and radiative deexcitation were taken into account by using data from [9] and [10], respectively.

Since the disk is thin and since the fraction of the solid angle in which the medium is optically thick is extremely small, $\Omega/4\pi \ll 1$, the maser amplification takes place only in a very narrow solid angle. We restrict ourselves to the case of an unsaturated maser, where the inverse effect of maser emission on signal level populations can be disregarded. This is confirmed, in particular, by the observed narrowness of the high-velocity line components. The above assumption allows us to "uncouple" the population-balance and radiative-transfer equations, i.e., to calculate the populations of ortho-H_2O levels locally at each point and to integrate the equations of radiative transfer by using the already known populations.

For a sufficiently homogeneous medium, the solution of the transfer equation is

$$I_\nu(\tau) = I_\nu(0)\exp(-\tau) + S_\nu^{ex}(1 - \exp(-\tau)), \tag{6}$$

where τ_ν is the optical depth at frequency ν:

$$\tau(R, \theta) = \int_{-\infty}^{\infty} \Phi_\nu(s) \frac{\lambda^2}{8\pi} g_2 A_{21} \left(\frac{n_1}{g_1} - \frac{n_2}{g_2}\right) ds, \tag{7}$$

$$\Phi_\nu(s) = \frac{1}{\sqrt{\pi}\Delta\nu_D} \exp\left(-\left(\frac{\nu - \nu_0(1 - V_s/c)}{\Delta\nu_D}\right)^2\right), \quad \Delta\nu_D = \frac{\nu_0 V_T}{c}, \tag{8}$$

where V_s is the line-of-sight velocity component. The emission intensity I_ν and the source function S_ν^{ex} in equation (6) can be expressed in terms of radiation temperature T_R and excitation temperature T_{ex}: $I_\nu = 2kT_R/\lambda^2$ and $S_\nu^{ex} = 2kT_{ex}/\lambda^2$.

Thus, in the case of normal absorption ($T_{ex} > 0, \tau > 0$), i.e., in the lines providing the radiative pumping of the maser, the radiation temperature averaged over the solid angle can be represented for a large optical depth as

$$\langle T_R \rangle = \frac{1}{4\pi} \int T_{ex}[1 - \exp(-\tau)] d\Omega \approx T_{kin} \frac{\Omega}{4\pi}. \tag{9}$$

In the case of negative absorption ($T_{ex} < 0, \tau < 0$), the maser radiation temperature is given by

$$T_R(\tau) = T_R(0)\exp|\tau| + |T_{ex}|(\exp|\tau| - 1), \tag{10}$$

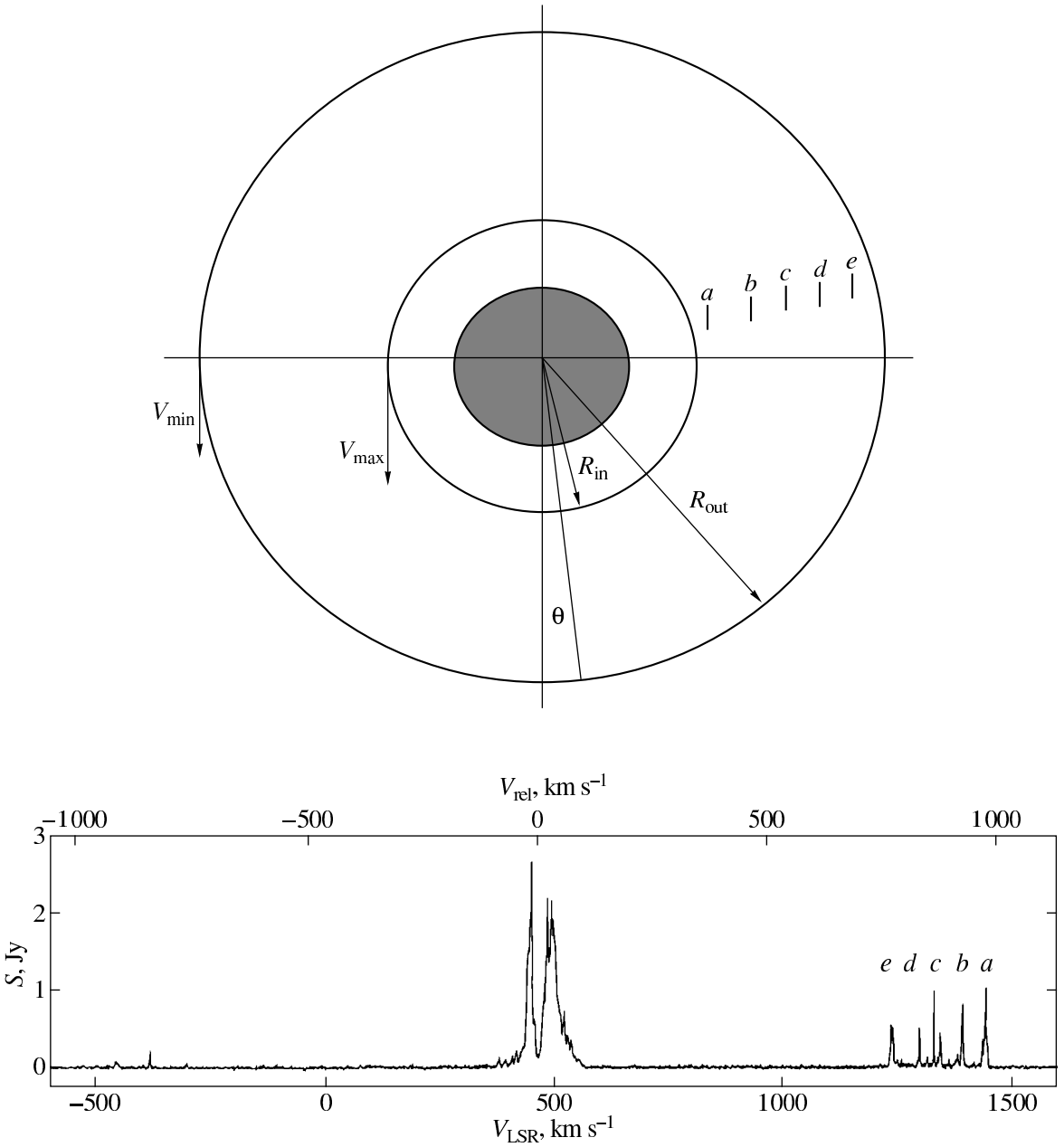

Fig. 1. A scheme of the molecular disk and the spectrum of maser emission in NGC 4258 [6] (published with permission of the authors).

where $T_R(0)$ is the brightness temperature of the ~22-GHz emission arising from the inner region and illuminating the maser.

A QUALITATIVE DESCRIPTION OF THE PUMPING MECHANISM

Figure 2 presents the results of an exact numerical calculation of the dependence of signal-level inversion

$$U = (n_u/g_u - n_l/g_l)/n_{H_2O} \quad (11)$$

for the ortho-H_2O molecule on hydrogen number density n_{H_2} and temperature T_{kin}.

Our numerical analysis has shown that, in the case under consideration, the RR radiative pumping mechanism is dominant. The main contribution to the emergence and magnitude of the inversion comes from the pumping cycle $4_{14} \longrightarrow 5_{05} \longrightarrow 6_{16} \longrightarrow 5_{23} \longrightarrow 4_{14}$. This cycle is schematically shown in Fig. 3.

The populations of the 6_{16}, 4_{14} and 5_{23}, 4_{14} levels are related by

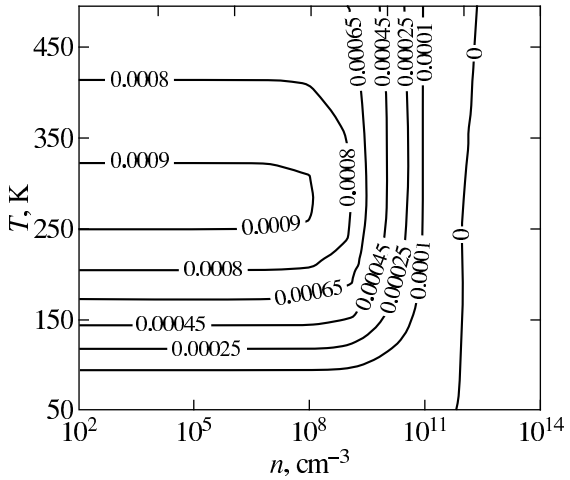

Fig. 2. Inversion U (11) of the populations of the 6_{16}–5_{23} signal levels in the ortho-H_2O molecule *versus* number density and temperature of molecular hydrogen.

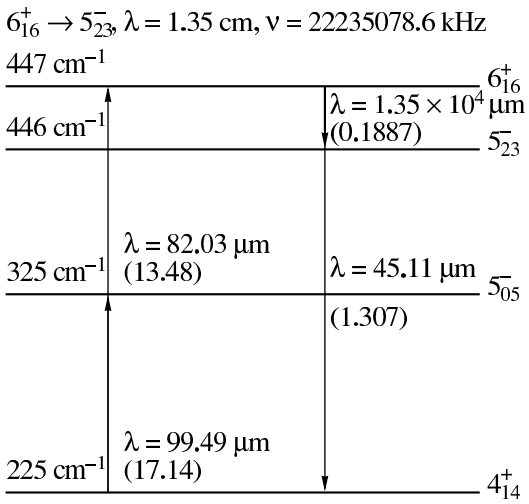

Fig. 3. A portion of the diagram of the ortho-H_2O rotational levels involved in the maser radiative pumping. The line oscillator strengths determining the optical depths and fluxes at the corresponding frequencies are given in parentheses.

$$\frac{n(6_{16})}{n(4_{14})} = \frac{n(6_{16})}{n(5_{05})}\frac{n(5_{05})}{n(4_{14})}$$

$$= \frac{g(6_{16})}{g(4_{14})}\exp\left(-\frac{\varepsilon(6_{16})-\varepsilon(5_{05})}{kT_R^{6_{16}\to 5_{05}}}\right)\exp\left(\frac{\varepsilon(5_{05})-\varepsilon(4_{14})}{kT_R^{5_{05}\to 4_{14}}}\right), \quad (12)$$

$$\frac{n(5_{23})}{n(4_{14})} = \frac{g(5_{23})}{g(4_{14})}\exp\left(-\frac{\varepsilon(5_{23})-\varepsilon(4_{14})}{kT_R^{5_{23}\to 4_{14}}}\right),$$

the radiation temperatures T_R^{ik} in these $i \longrightarrow k$ lines of the cycle satisfy the inequality $T_R^{4_{14}\to 5_{05}} \approx T_R^{5_{05}\to 6_{16}} \gg T_R^{5_{23}\to 4_{14}}$, because the oscillator strengths $\mu_{ik} \sim A_{ik}\lambda^3$ of the $4_{14} \longrightarrow 5_{05}$ and $5_{05} \longrightarrow 6_{16}$ transitions are a factor of 10 larger than that of the $5_{23} \longrightarrow 4_{14}$ transition. The optical depths in these transitions, determined by the corresponding values of μ_{ik}, are therefore related by $\tau_{4_{14}\to 5_{05}} \approx \tau_{5_{05}\to 6_{16}} \approx 10_{\tau_{5_{23}\to 4_{14}}}$.

Consequently, the fractions of the solid angles in which the medium is optically thick in the above lines are related by $\Omega^{4_{14}\to 5_{05}} \approx \Omega^{5_{05}\to 6_{16}} \gg \Omega^{5_{23}\to 4_{14}}$.

Thus, the radiation tends to excite molecules from the 4_{14} level (via the 5_{05} level) to the 6_{16} level and to deexcite the 5_{23} level through the transition to the 4_{14} level, forming a closed cycle of maser pumping and producing the signal-level inversion required for the maser amplification to emerge.

A detailed numerical calculation with allowance for all possible collisional and radiative transitions confirms that the main contribution to the pumping of maser levels comes from the mechanism considered in this section.

STRUCTURE OF THE MOLECULAR ACCRETION DISK

The critical distance at which ice particles in the Solar system are known to be completely destroyed by solar radiation is $\sim 1.5 \times 10^{13}$ cm. By analogy, we can estimate the critical distance of grain survival near the nucleus of the galaxy NGC 4258: $R_{BH}/R_\odot)^2 = (L_{BH}/L_\odot)$; for $L_{BH} = 10^{43}$ erg s^{-1}, $R_{BH} = 2 \times 10^{17}$ cm. At the distance corresponding to the inner disk radius, ice particles therefore survive even without obscuration by dust (which is very large, $A_V > 100$). The source of working H_2O molecules in the maser disk can thus be assumed to be ice dust.

According to observational data, the peak in the distribution of infrared radiation from the galaxy nucleus corresponds to a temperature of ~130 K. Since the most likely source of radiation in this wavelength range is dust, we conclude that the dust temperature is also ~130 K.

As the surface layers of the disk contain no dust responsible for gas cooling, the temperature in them is higher than the gas temperature in the central plane filled with dust; in addition, the hydrogen molecule is a factor of 9 less massive than the water molecule. We can therefore assert that the hydrogen atmosphere is much thicker than the layer containing H_2O molecules. The assumption that the diffusion flux of water molecules is low and that there is dynamical equilibrium on the dust surface is then valid, and we can use the satu-

rated-vapor equation for H_2O. In terms of the density of gas-phase H_2O molecules, this equation is

$$\log(n_{H_2O}(T_d)\ (\mathrm{cm}^{-3})) = a_1 - a_2/T_d + a_3\log T_d - a_4 T_d - a_5 T_d^2, \quad (13)$$

where $a_1 = 10.834292$, $a_2 = 2481.604$, $a_3 = 2.5721988$, $a_4 = 3.097203 \times 10^{-3}$, $a_5 = 1.7649 \times 10^{-7}$.

The maser emission intensity is extremely sensitive to the number density n_{H_2O} of working molecules. Since, according to observational data, the intensities of the high-velocity maser peaks originating at different distances from the center are approximately the same, $n_{H_2O}(R) \approx$ const in the maser disk. Because of the strong dependence of n_{H_2O} on T_d, we then conclude that $T_d(R) \approx$ const = 130 K for $R_{in} \le R \le R_{out}$.

CONSTRUCTING A MODEL FOR THE MOLECULAR DISK

When constructing a model for the molecular accretion disk, we follow Shakura and Sunyaev [11] but use a different equation of energy balance, because the mechanism of heating and heat removal in the molecular disk is markedly different.

Let us write the continuity equation integrated over the disk thickness $2H$ as

$$\dot{M} = 2\pi\Sigma R V_r, \quad (14)$$

where V_r is the mean radial velocity of the matter in the disk, and $\Sigma = 2H\rho$ is the surface density ($\rho = m_{H_2} n_{H_2}$).

We assume that the disk is in hydrostatic equilibrium: the pressure gradient is balanced by the z component of the gravity of the central body (the self-gravitation of the disk may be disregarded, because the disk mass is much smaller than the central mass):

$$\frac{1}{\rho}\frac{dP}{dz} = -\frac{GM}{R^3}z = -\omega^2 z, \quad (15)$$

where $\omega = \sqrt{GM/R^3}$ is the Keplerian angular velocity.

We integrate equation (15) and average it over z by using the equation of state $P = nkT$ (k is the Boltzmann constant). As a result, we obtain the following relation for the mean pressure in the disk

$$P = \frac{\Sigma\omega^2 H}{4}. \quad (16)$$

Without going into the details of the vertical disk structure, we rewrite equation (15) by assuming $\Delta P = \rho C_s^2$ (C_s is the speed of sound) and $\Delta z = H$ (disk half-thickness). We then have

$$C_s = \omega H. \quad (17)$$

Since, according to observational data, the radial component of the gas velocity is much smaller than its tangential component [2], we assume that the motion in the disk occurs in Keplerian circular orbits:

$$V_\varphi = \sqrt{\frac{GM}{R}} = \omega R. \quad (18)$$

Then, from formulas (17) and (18) it follows that

$$\frac{C_s}{V_\varphi} \approx \frac{H}{R}. \quad (19)$$

The radial motion in the disk is attributable to the friction of adjacent layers and to the exchange of angular momentum between them. The transfer of angular momentum in the disk is related to the moment of viscous forces by

$$\dot{M}\frac{d\omega R^2}{dR} = 2\pi\frac{d}{dR}W_{r\varphi}R^2, \quad (20)$$

where $W_{r\varphi}$ is the component of the viscous stresses in the disk

$$W_{r\varphi} = -2\eta HR\frac{d\omega}{dR}, \quad (21)$$

η is the dynamic viscosity coefficient averaged over the z coordinate. In the case of isotropic turbulence, the viscosity coefficient is [12]

$$\eta = \frac{1}{3}\rho v_t l_t, \quad (22)$$

where v_t and l_t are the characteristic velocity and scale of turbulent pulsations. The values of v_t and l_t in the accretion disk are not known in advance. This uncertainty can be obviated by assuming that $v_t l_t = \alpha C_s H$, where α is a dimensionless parameter, called the turbulence parameter. Clearly, $l_t \le H$ for isotropic turbulence. Since supersonic turbulence rapidly decays, $v_t \le C_s$. We therefore assume that $\alpha \le 1$.

Equation (20) for the change in angular momentum is easily integrated:

$$W_{r\varphi} = -\frac{\dot{M}}{2\pi}\omega\left(1 - \left(\frac{R_0}{R}\right)^{1/2}\right) + W_{r\varphi}(R_0), \quad (23)$$

where $W_{r\varphi}(R_0)$ is the component of the viscous stress tensor in an orbit of radius R_0.

When accretion onto a black hole is considered, the distance R_0 is assumed to correspond to the last stable orbit, $R_0 \sim R_g$ ($R_g \approx 10^{13}$ cm is the gravitational radius of the black hole). The subsequent radial motion of the matter to the black hole takes place through general-relativity effects, so that $W_{r\varphi}(R_0) = 0$. Then, from (23) for $R \gg R_0$, we have

$$W_{r\varphi} \approx -\frac{\dot{M}}{2\pi}\omega, \quad (24)$$

and, by the definition of $W_{r\varphi}$ (21),

$$W_{r\varphi} \simeq 3\eta H\omega = \alpha PH. \quad (25)$$

Let us write the equation of energy balance. For the dust-filled layers near the central plane of the disk, we obtain

$$\frac{d}{dz}\lambda\frac{dT}{dz}-\eta R^2\left(\frac{d\omega}{dR}\right)^2-\frac{L_x}{4\pi R^2}\zeta_\nu n_H+4\pi l^2 n_d\sigma T_d^4=0, \quad (26)$$

where λ is the coefficient of heat conductivity for hydrogen, n_d is the dust number density, l is the grain radius, L_x is the luminosity of X-ray emission incident on the inner boundary of the maser disk, and ζ_ν is the frequency-dependent cross section of photoionization by X-ray emission [13].

The low-frequency part of the X-ray spectrum is absorbed most effectively by hydrogen at distances smaller than R down to the frequency determined from the condition $\tau_\nu = n_{H_2}\zeta_\nu R \sim 1$. Then, we rewrite equation (26) as

$$\frac{d}{dz}\lambda\frac{dT}{dz}-\frac{9}{4}\eta\omega^2-\frac{L_x}{4\pi R^3}+4\pi l^2 n_d\sigma T_d^4 = 0. \quad (27)$$

For the disk upper layers, the equation of energy balance takes the form

$$\frac{d}{dz}\lambda\frac{dT}{dz}-\frac{9}{4}\eta\omega^2-\frac{L_x}{4\pi R^3} = 0. \quad (28)$$

Let us average equation (27) using relation (21):

$$\frac{d}{dz}\lambda\frac{dT}{dz}-\frac{3W_{r\varphi}\omega}{4H}-\frac{L_x}{4\pi R^3}+4\pi l^2 n_d\sigma T_d^4 = 0. \quad (29)$$

Given that $\lambda = 5/2\eta C_V = 5/6 C_V\rho\alpha C_s H$ and that the speed of sound $C_s = \sqrt{\gamma kT/m_{H_2}}$ (m_{H_2} is the mass of the hydrogen molecule), we integrate equation (29) over the vertical z coordinate:

$$\frac{5}{18}C_V\alpha\Sigma\sqrt{\frac{\gamma k}{m_{H_2}}}\Delta T^{3/2}-\frac{3}{4}W_{r\varphi}\omega\frac{z^2}{H}-\frac{L_x z^2}{4\pi R^3} + 4\bar{n}_d\pi\bar{l}^2\sigma T_d^4 z^2 = 0. \quad (30)$$

Assuming the dust surface density to be $2\bar{n}_d H = 0.01\Sigma/m_d$ (m_d is the mass of a single dust grain), we have the following relation for energy balance:

$$\frac{5}{18}C_V\alpha\Sigma\sqrt{\frac{\gamma k}{m_{H_2}}}\Delta T^{3/2}-\frac{3}{4}W_{r\varphi}\omega\frac{z^2}{H} -\frac{L_x z^2}{4\pi R^3}+0.02\pi\bar{l}^2\frac{\Sigma}{m_d H}\sigma T_d^4 z^2 = 0. \quad (31)$$

Similarly, for the dust-free layers of gas, we obtain

$$\frac{5}{18}C_V\alpha\Sigma\sqrt{\frac{\gamma k}{m_{H_2}}}\Delta T^{3/2}-\frac{3}{4}W_{r\varphi}\omega\frac{z^2}{H}-\frac{L_x z^2}{4\pi R^3} = 0. \quad (32)$$

Let us introduce the following dimensionless parameters

$$r = \frac{R}{R_{out}},\quad \xi = \frac{z}{H(r)},$$
$$m = \frac{M}{4\times 10^7 M_\odot},\quad \dot{m} = \frac{\dot{M}}{10^{-4}M_\odot\ \mathrm{yr}^{-1}}. \quad (33)$$

Numerical simulations show that the dependence of gas temperature $T(r, \xi)$ at height H can be fitted by a second-degree polynomial,

$$T(r, 1) = T(1, 1)(1 + a(1-r) + b(1-r)^2), \quad (34)$$

where a and b are the polynomial coefficients. As a result, we obtain the following set of relations for the main disk parameters in the range $R_{in} \le R \le R_{out}$:

$$H = 1.1\times 10^{15}(1 + a(1-r) + b(1-r)^2)^{1/2} m^{-1/2} r^{3/2}\ \mathrm{cm},$$
$$\Sigma = 3.7\times 10\alpha^{-1}(1 + a(1-r) + b(1-r)^2)^{-1}\dot{m}m^{1/2}r^{-3/2}\ \mathrm{g\ cm^{-2}},$$
$$V_\varphi = 7.8\times 10^7 m^{1/2} r^{-1/2}\ \mathrm{cm\ s^{-1}},$$
$$V_r = 1.2\times 10^2\alpha(1 + a(1-r) + b(1-r)^2)m^{-1/2}r^{1/2}\ \mathrm{cm\ s^{-1}},$$
$$\rho = 1.7\times 10^{-14}\alpha^{-1}(1 + a(1-r) + b(1-r)^2)^{-3/2}\dot{m}mr^{-3}\ \mathrm{g\ cm^{-3}},$$
$$P = 8.2\times 10^{-5}\alpha^{-1}(1 + a(1-r) + b(1-r)^2)^{-1/2}\dot{m}mr^{-3}\ \mathrm{dyne\ cm^{-2}}. \quad (35)$$

The temperature profile $T(r, \xi)$ can be represented as

$$T = T(r, 0)\left(1 + \frac{\xi^2}{r^{-\delta}}\left(0.63(1 + a(1-r) + b(1-r)^2)^{3/2} + \frac{(1 + a(1-r) + b(1-r)^2)^2}{100\dot{m}m^{3/2}r^{-3/2}}\right)\right)^{2/3}\ \mathrm{K}, \quad (36)$$

where $T(r, 0) = T_d(r) = T_d^{out} r^{-\delta}$ (T_d^{out} is the dust temperature at the outer radius of the maser disk).

The best agreement between the observed profile of the maser emission and the calculations was achieved for the following model parameters: $M = 3.8\times 10^7 M_\odot$; $\dot{M} = 10^{-4}M_\odot\ \mathrm{yr}^{-1}$; $\alpha = 0.2$; the radiation energy of the central source absorbed by the maser disk, $L_x = 10^{39}\ \mathrm{erg\ s^{-1}}$, for a total X-ray luminosity of the central source $4.1\times 10^{40}\ \mathrm{erg\ s^{-1}}$ in the 3–10-keV band; the brightness temperature of the central source at ~22 GHz $T_R = 2\times 10^6$ K [14]; the dust temperature $T_d(r) = T_d^{out} r^{-\delta} = 130 r^{-0.0625}$ K; and

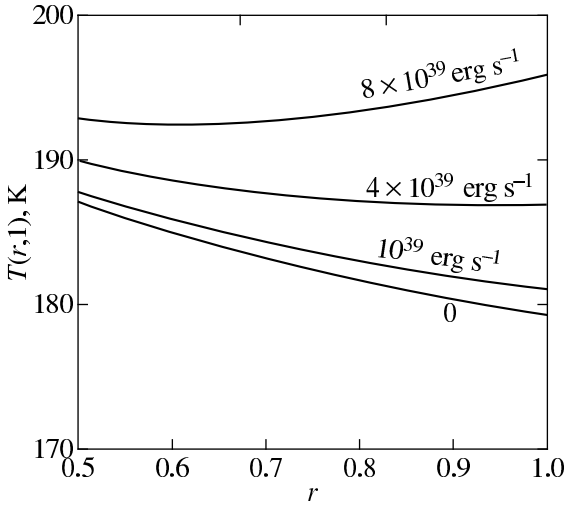

Fig. 4. Gas temperature at height $z = H$ *versus* distance $r = R/R_{out}$ for various X-ray luminosities L_x heating the maser disk.

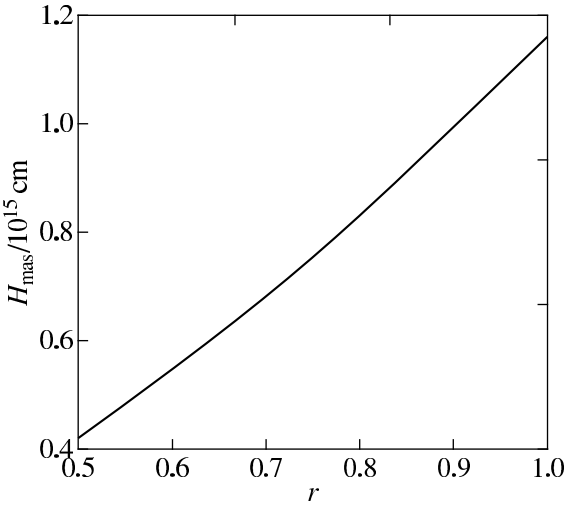

Fig. 5. Maser-layer height H_{mas} *versus* dimensionless radius $r = R/R_{out}$.

the disk recession velocity 474 km s^{-1}. For these parameters, the coefficients in (34) are $a = 0.040$ and $b = 0.067$ (Fig. 4).

The dependence of maser-layer height H_{mas} on disk radius is shown in Fig. 5. Since the thickness of the maser layer is $\approx 10^{12}$ cm and its height is $H_{mas} \sim H$, the layer temperature is $T_{mas} \approx T(r, 1)$.

Our model allows both the spectral line profile and the fluxes F_ν in various components to be obtained, which are in excellent agreement with observational data (Fig. 6), $F_\nu = I_\nu \pi \Theta^2$ ($\Theta = 4 \times 10^{-11}$ rad is the effective size of the maser feature [2]).

PECULIARITIES OF THE STRUCTURE OF THE MASER LINE PROFILE

Since the radial component of the gas velocity in the disk is much smaller than its tangential component, the velocity field can be assumed to obey Kepler's law (1). According to Grinin and Grigor'ev [15], at each point R, there are two directions, s^+ and s^-, making angles θ_+ and θ_- with the extension of the radius vector **R**, along which the velocity gradient is zero. In the case of a purely Keplerian velocity field in the disk plane, $\theta_+ = 0$ and $\theta_- = 90°$.

Since relation (7) for the optical depth $\tau(R, \theta)$ contains an exponential velocity profile $\Phi_\nu(s)$, the exponent in (8) strongly affects the emission intensity and, consequently, the structure of the spectrum.

Let us expand the expression in (8) in a power series of s:

$$\frac{\nu - \nu_0(1 - V_s/c)}{\Delta\nu_D} = \frac{s}{V_t}\frac{dV_s}{ds} + \frac{s^2}{2V_t}\frac{d^2V_s}{ds^2} + \ldots . \quad (37)$$

We then see from relation (37) that the coherent length s_0 is at a maximum in directions close to s^+ and s^- (s_0 is the distance at which the emission emerges from resonance, shifting by $\Delta\nu_D$). Since $\tau(R, \theta) \propto s_0(R, \theta)$,

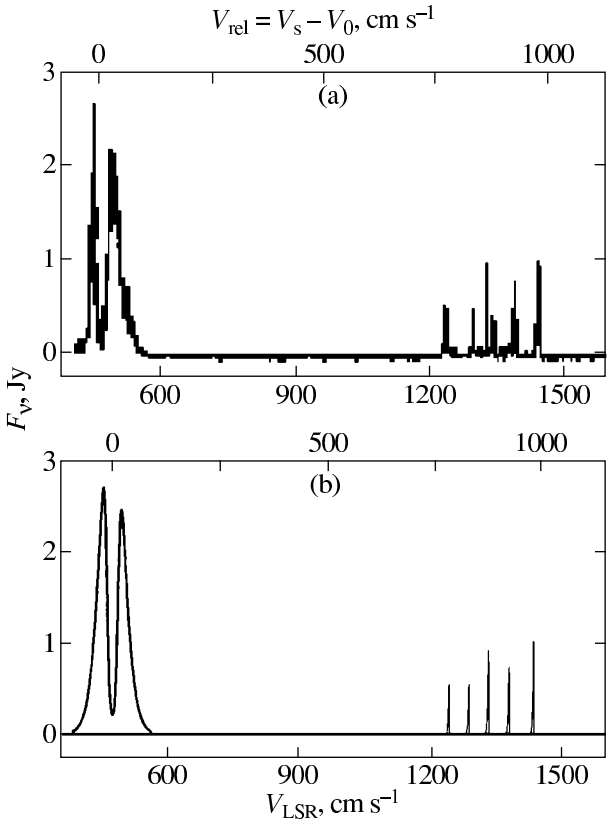

Fig. 6. The spectrum of H_2O maser emission from the nucleus of the galaxy NGC 4258: (a) results of the observations [6] (published with permission of the authors); (b) results of the numerical simulations (this study).

the maser emission intensity in the maser amplification mode peaks in these directions.

The coherent length at angles θ close to θ_+ is limited by the sizes of the maser disk; at other values of θ, s_0 is given by [15]

$$s_0(R, \theta) = s_{1/2}(R, \theta) + s_{1/2}(R, \theta + \pi), \quad (38)$$

where $s_{1/2}$ is the distance from the point **R** at which the resonance-frequency shift is $\Delta\nu_D/2$. This distance can be determined from the equation

$$\left| \frac{s}{V_t}\frac{dV_s}{ds} + \frac{s^2}{2V_t}\frac{d^2V_s}{ds^2} + \ldots \right| = \frac{1}{2}. \quad (39)$$

Figure 7 shows a plot of dimensionless coherent length $s_0/(R_{out} - R_{in})$ against angle θ with allowance for the first three terms of the V_s expansion in (37) for an absolutely flat disk and a line of sight parallel to the disk plane. This figure accounts for the observational fact that there are central and high-velocity components in the maser spectrum and no visible emission at intermediate velocities.

However, the disk plane may be curved by flexural waves. The hypothesis about the existence of such waves is based on the discrete regular structure of the high-velocity components in the maser spectrum, because flexural waves produce a continuous change in the inclination of the disk plane to the observer. Thus, it would be natural to assume that the line of sight lies in the disk plane for the high-velocity components in some directions; in this case, the coherent length of the ray path, $s_0 \simeq 2 \times 10^{15}$ cm, is much smaller than the radius of curvature of the disk ($s_0 \ll R$).

It follows from observational data that the width of the high-velocity components is ~5 km s^{-1}. Numerical simulations show that such a broadening arises at $\theta \approx \theta_- + 3°$ (or $\theta \approx \theta_- - 3°$). This result also suggests that there are spiral flexural waves in the maser disk. Furthermore, the spiral pattern of flexural waves explains the asymmetry of the high-velocity components in the right and left parts of the spectrum.

According to observational data, the width of the central spectral component is $\delta\theta \approx 14°$. If we assume the existence of flexural waves with ~3 crests in the segment between the inner and outer disk radii (which corresponds to five high-velocity maser peaks) and amplitude $A \geq (R_{out} - R_{in})/(10\tan i_0)$, where i_0 is the inclination of the disk spin axis to the observer, $i_0 = 97° \pm 4°$, [7], then there will always be such a location of the ray for which the inclination of the disk plane to the observer is nearly zero. In this case, the coherent length of the ray path is $s_0 \ll (R_{out} - R_{in})/10$. Numerical simulations show that, for the above ray location and for the maser-layer thickness $h = 10^{12}$ cm, the inclination of the disk plane to the observer is ≈0.022° ($s_0 \approx 2.6 \times 10^{15}$ cm).

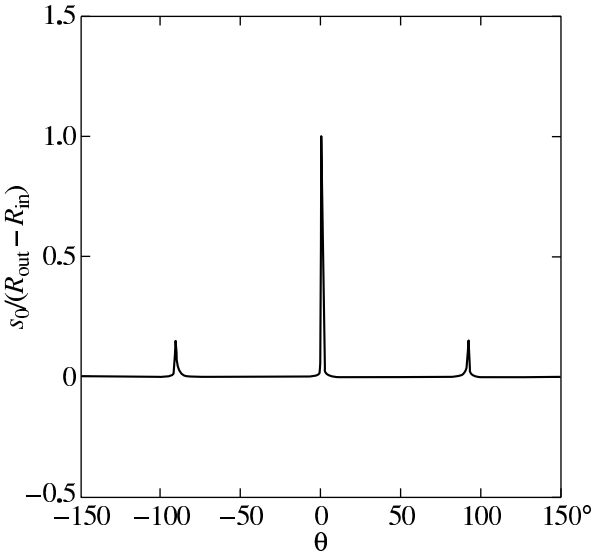

Fig. 7. Coherent length $s_0/(R_{out} - R_{in})$ *versus* angle θ.

The splitting of the central spectral component can be explained by the presence of an absorbing region containing H_2O molecules on the line of sight. According our calculations, the optical depth τ of this region in the H_2O line is 3, the turbulent velocity is 11 km s^{-1}, and the recession velocity is 476 km s^{-1}.

CONCLUSION

Based on our numerical calculations of the population kinetics of ortho-H_2O molecular rotational levels with allowance for detailed data on the probabilities of radiative and collisional transitions between 30 lower rotational levels of ortho-H_2O, we have elucidated the optimal conditions for the emergence of an inverse population of the signal 6_{16}–5_{23} levels and effective maser amplification of the λ = 1.35 cm line emission. The strong dependence of maser intensity on the number density and temperature of the H_2 buffer gas and H_2O working molecules allowed us to determine, with a sufficiently high accuracy, the density and temperature profiles of the gas in the gas–dust accretion disk and the parameters of the medium in which the amplification takes place. Under the derived conditions, we elucidated the most probable mechanism of maser pumping in a molecular accretion disk differentially rotating around a black hole of mass $M = (4.0 \pm 0.25) \times 10^7 M_\odot$ (D/7.3 Mpc) at the accretion rate $\dot{M} = 10^{-4} M_\odot$ yr^{-1} (D/7.3 Mpc)^2.

By analyzing observational data, we determined the key model parameters: the radiation energy of the central source absorbed by the maser disk, $L_x = 10^{39}$ erg s^{-1}, turbulence parameter $\alpha \simeq 0.2$, brightness temperature of the central source at ~22 GHz $T_R = 2 \times 10^6$ K, disk

recession velocity 474 km s^{-1}, and dust temperature $T_d = T_d^{out} r^{-\delta} = 130 r^{-0.0625}$ K.

Taking into account the spiral flexural waves in the disk, we calculated the multicomponent spectral-line profile; the derived absolute fluxes of individual line components are in good agreement with observational data.

ACKNOWLEDGMENTS

This study was supported by the Russian Foundation for Basic Research (project code 99-02-18232), the Russian Ministry of Education (project MO 021-00-2-02) and ESO CSEE (grant no. B-04-062).

REFERENCES

1. C. F. Gammie, R. Narayan, and R. Blandford, Astrophys. J. **516**, 177 (1999).
2. M. Miyoshi, J. Moran, J. Herrnstein, *et al.*, Nature **373**, 127 (1995).
3. G. Courtes, H. Petit, C. T. Hua, *et al.*, Astron. Astrophys. **268**, 419 (1993).
4. B. J. Wilkes, G. D. Schmidt, P. S. Smith, *et al.*, Astrophys. J. Lett. **455**, L13 (1995).
5. M. J. Claussen, G. M. Heiligman, and K. Y. Lo, Nature **310**, 298 (1984).
6. N. Nakai, M. Inoue, and M. Miyoshi, Nature **361**, 45 (1993).
7. J. Moran, L. Greenhill, P. Diamond, *et al.*, Proc. Natl. Acad. Sci. USA **92**, 1147 (1995).
8. G. Cecil, A. S. Wilson, and R. B. Tully, Astrophys. J. **390**, 365 (1992).
9. G. Piehler, D. A. Varshalovich, V. K. Khersonskiĭ, *et al.*, Astron. Astrophys., Suppl. Ser. **76**, 195 (1988).
10. S. Chandra, D. A. Varshalovich, and W. H. Kegel, Astron. Astrophys., Suppl. Ser. **55**, 51 (1984).
11. N. I. Shakura and R. A. Sunyaev, Astron. Astrophys. **24**, 337 (1973).
12. L. D. Landau and E. M. Lifshitz, *Mechanics of Continuous Media* (Gostekhizdat, Moscow, 1953).
13. V. B. Berestetskiĭ, E. M. Lifshitz, and L. P. Pitaevskiĭ, *Quantum Electrodynamics* (Nauka, Moscow, 1980).
14. J. R. Herrnstein, L. J. Greenhill, J. M. Moran, *et al.*, Astrophys. J. Lett. **497**, L69 (1998).
15. V. P. Grinin and S. A. Grigor'ev, Astron. Zh. **60**, 512 (1983).

Translated by G. Rudnitskii